Large Graphene Quantum Dots Alleviate Immune-Mediated Liver Damage

Vladislav Volarevic,[†,⊗] Verica Paunovic,[‡,⊗] Zoran Markovic,[⊥,⊗] Bojana Simovic Markovic,[†] Maja Misirkic-Marjanovic,[‡,§] Biljana Todorovic-Markovic,[⊥] Sanja Bojic,[†] Ljubica Vucicevic,[‡,§] Svetlana Jovanovic,[⊥] Nebojsa Arsenijevic,[†] Ivanka Holclajtner-Antunovic,[#] Momir Milosavljevic,[⊥] Miroslav Dramicanin,[⊥] Tamara Kravic-Stevovic,[∥] Darko Ciric,[∥] Miodrag L. Lukic,[*,†] and Vladimir Trajkovic[*,‡]

[†]Centre for Molecular Medicine and Stem Cell Research, Faculty of Medical Sciences, University of Kragujevac, 69 Svetozara Markovica Street, 34000 Kragujevac, Serbia, [‡]Institute of Microbiology and Immunology, School of Medicine, University of Belgrade, Dr Subotica 1, 11000 Belgrade, Serbia, [§]Institute for Biological Research, University of Belgrade, Despota Stefana Boulevard 142, 11000 Belgrade, Serbia, [⊥]Vinca Institute of Nuclear Sciences, University of Belgrade, P.O. Box 522, 11000 Belgrade, Serbia, [∥]Institute of Histology and Embriology, School of Medicine, University of Belgrade, Visegradska 26, 11000 Belgrade, Serbia, and [#]Faculty of Physical Chemistry, University of Belgrade, Studentski trg 12-16, 11000 Belgrade, Serbia. [⊗]These authors contributed equally.

ABSTRACT We investigated the effect of large (40 nm) graphene quantum dots (GQDs) in concanavalin A (Con A; 12 mg/kg i.v.)-induced mouse hepatitis, a T cell-mediated liver injury resembling fulminant hepatitis in humans. Intravenously injected GQDs (50 mg/kg) accumulated in liver and reduced Con A-mediated liver damage, as demonstrated by histopathological analysis and a decrease in liver lipid peroxidation and serum levels of liver transaminases. The cleavage of apoptotic markers caspase-3/PARP and mRNA levels of proapoptotic mediators Puma, Noxa, Bax, Bak1, Bim, Apaf1, and p21, as well as LC3-I conversion to autophagosome-associated LC3-II and expression of autophagy-related (Atg) genes Atg4b, Atg7, Atg12, and beclin-1, were attenuated by GQDs, indicating a decrease in both apoptosis and autophagy in the liver tissue. This was associated with the reduced liver infiltration of immune cells, particularly the T cells producing proinflammatory cytokine IFN-γ, and a decrease in IFN-γ serum levels. In the spleen of GQD-exposed mice, mRNA expression of IFN-γ and its transcription factor T-bet was reduced, while that of the IL-33 ligand ST2 was increased. The hepatoprotective effect of GQDs was less pronounced in ST2-deficient mice, indicating that it might depend on ST2 upregulation. *In vitro*, GQDs inhibited splenocyte IFN-γ production, reduced the activation of extracellular signal-regulated kinase in macrophage and T cell lines, inhibited macrophage production of the free radical nitric oxide, and reduced its cytotoxicity toward hepatocyte cell line HepG2. Therefore, GQDs alleviate immune-mediated fulminant hepatitis by interfering with T cell and macrophage activation and possibly by exerting a direct hepatoprotective effect.

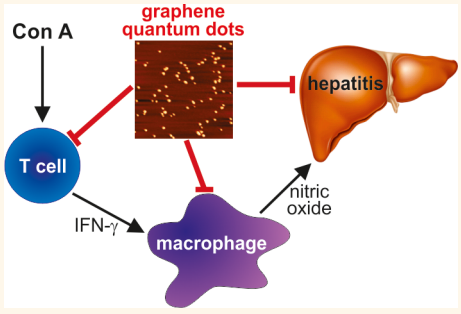

KEYWORDS: graphene · quantum dot · hepatitis · apoptosis · autophagy

Graphene, the most recently discovered carbon allotrope consisting of a single layer of carbon atoms in a honeycomb structure, has gained considerable attention in nanomedicine as a potential diagnostic and therapeutic tool.[1−3] Graphene quantum dots (GQDs) are graphene sheets with lateral dimensions less than 100 nm containing one or more (2−10) graphene layers.[4,5] Although most of the top-down methods yield GQDs with sub-10 nm diameter, larger GQDs of up to 60 nm diameter have also been synthesized by using various top-down or bottom-up approaches.[5,6] While sharing the graphene's ultrahigh surface area for bioconjugation, GQDs additionally possess the edge defects that endow them with tunable, size/wavelength-dependent luminescence potentially useful in bioimaging.[5,6] Due to a different electronic structure compared to parental semimetal graphene, semiconductor GQDs display some unique physicochemical properties and, because of their superior chemical inertness and biocompatibility, represent low-toxicity alternatives of conventional QDs (*e.g.*, CdSe). In addition to their excellent photoluminescent properties, GQDs can act both as electron donors and electron acceptors,[7] which indicates their prooxidant as well as antioxidant potential. Accordingly, laser ablation-generated, poly(ethylene glycol)-passivated GQDs produce reactive oxygen species (ROS) upon irradiation with blue light, while in the absence of photoexcitation they display a potent ROS-quenching ability.[8]

* Address correspondence to vtrajkovic@med.bg.ac.rs, miodrag.lukic@medf.kg.ac.rs.

Received for review May 6, 2014 and accepted November 21, 2014.

Published online November 21, 2014
10.1021/nn502466z

ROS production regulates the function and activity of immune cells.[9] ROS generation in activated T cells is required for optimal induction of transcription factors NFAT and NF-κB and subsequent cytokine production and clonal expansion of T cells.[10,11] Excessive ROS release by macrophages can cause DNA damage in neighboring cells, resulting in inflammatory damage of various tissues, including liver.[12−14] It is therefore plausible to assume that ROS modulation by GQDs might interfere with the T cell and macrophage function during inflammation and autoimmunity. However, while other carbon allotropes (fullerenes and nanotubes), and recently graphene, have displayed some immunomodulatory properties in different experimental systems,[15−24] the effects of GQDs on either normal or pathologic immune responses have not been explored so far. We here for the first time report the immunomodulatory and cytoprotective effects of GQDs in a mouse model of immune-mediated liver damage.

RESULTS AND DISCUSSION

To assess the therapeutic effect of GQDs in hepatitis, we decided to use large GQDs, as nanoparticles with diameter >10 nm are more likely to accumulate in the liver after intravenous injection[25] either *via* transvascular flow across the open sinusoidal fenestrae or upon transvascular release following phagocytosis by reticuloendothelial cells and hepatic Kupffer macrophages.[26] Furthermore, the use of large nanoparticles is preferable in treatment of inflamed tissues, which generally present with leaky blood vessels that, as opposed to the vasculature in healthy tissues, allow for the selective extravasation of nanomaterials with sizes of up to 400 nm.[27] Accordingly, GQDs with diameter ~5 nm accumulated less and/or equally in liver compared to kidneys,[28,29] while those larger than 10 nm accumulated markedly more in liver than in kidneys.[30] Moreover, a direct comparative study of GQDs with diameters of 5, 7, 12, and 21 nm revealed a positive correlation between their size and the accumulation in liver tissue.[31] Therefore, as in our previous studies,[32,33] we used electrochemical oxidation of graphite to produce GQDs of approximately 40 nm average length (20−67 nm) and 3 nm average height, corresponding to three graphene layers, as revealed by atomic force microscopy (AFM) (Figure 1A, upper panel). The high-resolution transmission electron microscopy (TEM) showing the edge structure of GQDs (Figure 1A, lower panel) indicates their high crystallinity, with a lattice parameter of 0.263 nm. From the photoluminescence spectra presented in Figure 1B it could be seen that GQDs emit bright blue luminescence upon excitation at 328 nm, displaying a strong peak at 504 nm with a Stokes shift of 176 nm. Similar to most luminescent carbon nanoparticles, GQDs exhibit an excitation-dependent photoluminescence behavior.[34] Accordingly, when the excitation wavelength is changed from 328 nm to 375, 417, or 469 nm, the photoluminescence peak shifts to longer wavelengths (496, 494, or 549 nm, respectively), and its intensity decreases rapidly (Figure 1B). The Raman spectroscopy analysis demonstrated two prominent bands, the D band at 1350 cm^{-1} and the G band at 1594 cm^{-1} (Figure 1C), corresponding to the in-plane A1g zone-edge mode and E2g mode, respectively.[35] We have employed this feature to trace GQDs in different tissues upon intravenous injection to mice. While no Raman peaks could be observed in the control sample of mouse liver, the liver tissue from GQD-injected mice readily displayed GQD-specific D and G bands, although they were slightly down-shifted (9 and 11 cm^{-1}, respectively) (Figure 1D). However, these bands were not present in the Raman spectra of brain, spleen, lung or kidney tissues of GQD-treated mice (Supporting Information, Figure S1). In addition to confirming that the synthesized carbon nanoparticles display specific characteristics of GQDs, our data demonstrate their accumulation in liver upon intravenous administration. This is consistent with the previous studies that reported accumulation of carboxylated and polydopamine-coated GQDs in the liver.[28−30] It should be noted that for biodistribution studies, in order to increase GQD-specific Raman signals over the tissue background signal, we used 2-fold higher dose of GQDs (100 mg/kg) than for the assessment of their hepatoprotective effect (50 mg/kg).

The effect of GQDs was tested in mouse hepatitis induced by intravenous injection of lectin Concanavalin A (Con A), which causes acute inflammatory liver injury resembling fulminant hepatitis in humans and involving both T cells and natural killer (NK)T cells.[36−38] A single intravenous administration of GQDs (50 mg/kg) significantly reduced Con A-induced liver damage, as confirmed by a decrease in serum levels of hepatic enzymes alanine aminotransferase (ALT) and aspartate aminotransferase (AST) (Figure 2A). Accordingly, histopathological analysis demonstrated that the liver tissue loss and inflammatory cell infiltration in Con A-treated mice were markedly reduced by GQD treatment (Figure 2B). The decrease in the levels of malondialdehyde (Figure 2C), an indicator of lipid peroxidation,[39] suggests that the hepatoprotective effect of GQDs was associated with the suppression of oxidative stress. As both apoptosis (programmed cell death type I) and autophagy (programmed cell death type II)[40] are responsible for Con A-induced liver injury,[41−43] we examined the influence of GQDs on the principal markers of these two cell death modes and the expression of major apoptosis/autophagy-regulating genes in Con A hepatitis. The immunoblot-detected activation of the key apoptosis-executing enzyme caspase-3 and subsequent cleavage of the DNA-repairing protein poly(ADP ribose) polymerase (PARP)[40] in Con A-injected mice were significantly downregulated by

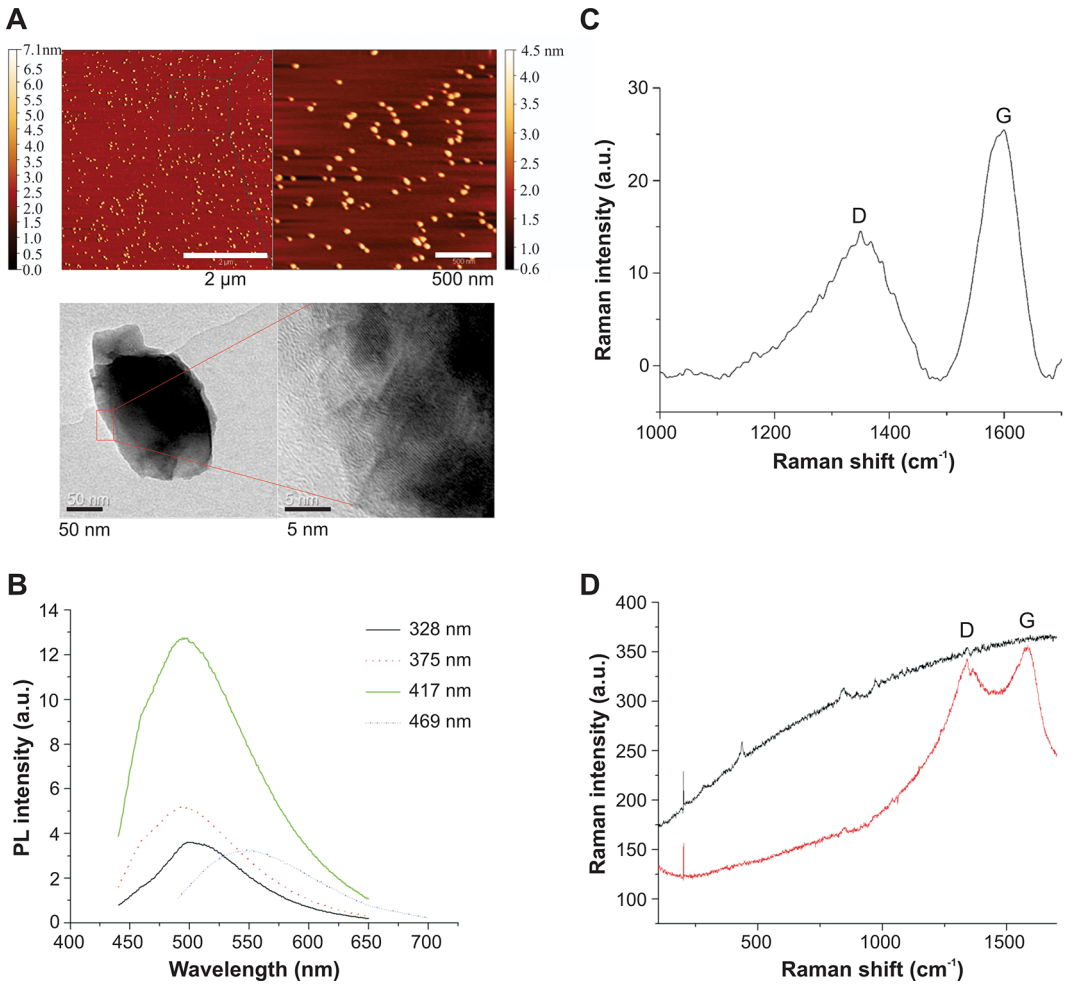

Figure 1. GQD characterization and liver accumulation. (A) Top view AFM images (upper panel) as well as low-resolution (lower left) and high-resolution (lower right) TEM images of GQDs are shown. (B) Photoluminescence spectra of GQDs at different excitation wavelengths. (C) Raman spectra of GQDs with the characteristic D and G bands at 1350 and 1594 cm^{-1}, respectively. (D) Raman spectra of mouse liver tissue collected 2 h after a single intravenous injection of saline (black line) or 100 mg/kg GQD (red line).

GQDs (Figure 2D). The induction of autophagy by Con A, demonstrated by the conversion of microtubule-associated protein 1 light-chain 3 (LC3)-I to autophagosome-associated LC3-II,[40] was markedly attenuated by GQDs (Figure 2D). Accordingly, a real-time RT-PCR analysis of liver tissue from Con A-exposed mice revealed that GQDs significantly reduced the expression of mRNA encoding proapoptotic mediators p21, Puma, Noxa, Bax, Bak1, Bim, and Apaf1 (Figure 2E). The expression of other proapoptotic (p27, Pten, Bad, p53) as well as antiapoptotic genes (Bcl-2, Bcl-xL, survivin, XIAP) was not significantly affected by GQDs (Figure 2E). The expression of autophagy-related (Atg) genes Atg4b, Atg7, Atg12, and beclin-1, which are all required for optimal induction of autophagy,[40] was also lower in Con A-treated mice that received GQDs. The difference in Atg5 and Gabarap levels did not reach statistical significance (Figure 2F). These data indicate that GQDs could alleviate Con A hepatitis through suppression of both apoptotic and autophagic hepatocyte demise.

The liver damage in Con A hepatitis is initiated by the infiltration of activated immune cells, so we next used flow cytometry to examine the effect of GQD administration on the hepatic influx of inflammatory cells. In accordance with the histological analysis showing smaller inflammatory infiltrates upon GQD treatment (Figure 2B), significantly lower numbers of $CD3^+$ (both $CD4^+$ and $CD8^+$) T cells (Figure 3A), $NK1.1^+$ NK cells, $CD11c^+$ dendritic cells (Figure 3B), $F480^+$ macrophages, and $CD19^+$ B cells (Figure 3C) were recovered from the liver tissue of GQD-injected animals with Con A hepatitis. $CD4^+$ T cells producing proinflammatory cytokines interferon (IFN)-γ and tumor necrosis factor (TNF), as well as interleukin (IL)-4-producing NKT cells seem to be the main culprits responsible for Con A-mediated liver inflammation and injury.[37,44,45] Accordingly, we found significantly lower numbers of $CD4^+$IFN-γ^+ and $CD8^+$IFN-γ^+ cells in the liver of Con A + GQD-treated mice compared to those treated with Con A alone (Figure 3D). While we observed a tendency of GQD to reduce the liver infiltration of $CD4^+$ T cells

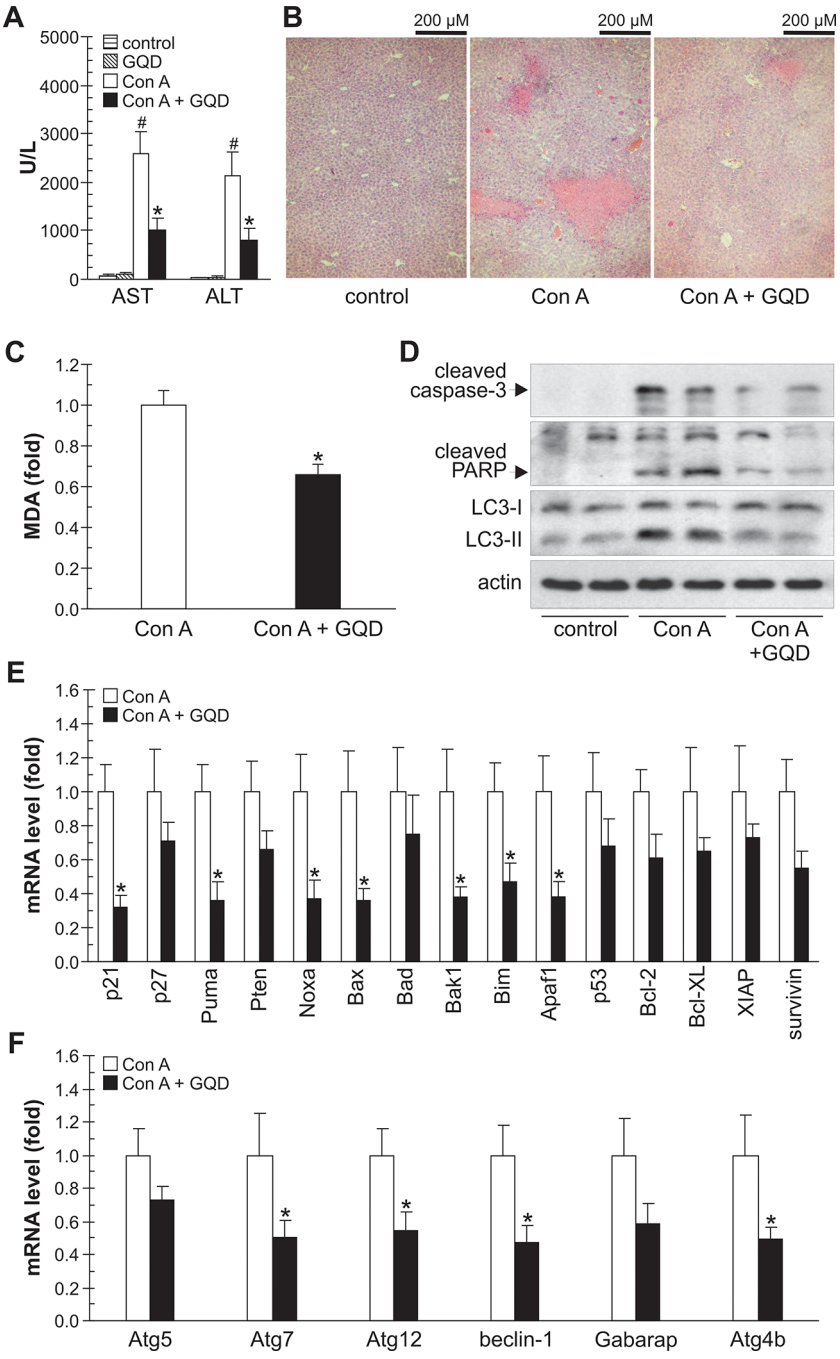

Figure 2. GQDs suppress Con A hepatotoxicity by reducing oxidative stress, apoptosis, and autophagy. (A–F) Single intravenous injection of GQDs (50 mg/kg) significantly reduces Con A-induced increase in serum levels of liver transaminases (A), liver tissue loss and inflammatory infiltration (B), lipid peroxidation (MDA, malondialdehyde) (C), as well as the expression of proapoptotic and autophagy-related proteins (D) and genes (E, F), measured 24 h (A–C) or 8 h (D–F) after the induction of hepatitis. The results of one of two experiments with similar results are presented as mean ± SEM values (n = 8 mice per group; $p^{\#} < 0.05$ compared to untreated control; $p^{*} < 0.05$ compared to Con A alone). Representative immunoblots are presented in (D).

producing IL-4 or IL-10 (Supporting Information, Figure 2A) and NKT ($CD3^{+}NK1.1^{+}$) cells producing IFN-γ, IL-4, TNF, or IL-10 (Supporting Information, Figure 2B), these differences did not reach statistical significance. In addition, the numbers of TNF-producing $CD4^{+}$ T cells and $CD4^{+}$ T regulatory cells ($CD25^{+}Foxp3^{+}$) did not differ between the two experimental groups (Supporting Information, Figure 2A). The reduction in numbers of infiltrating T cells producing IFN-γ (Figure 3D) was associated with a decrease in serum concentrations of this cytokine, but not TNF, IL-4, or IL-10 (Figure 3E). Accordingly, the expression of mRNA for IFN-γ and transcription factor T-bet, required for differentiation of IFN-γ-producing T helper (Th)1 cells,[46,47] was lower in the spleen of GQD-treated animals (Figure 3F). The expression of mRNA encoding

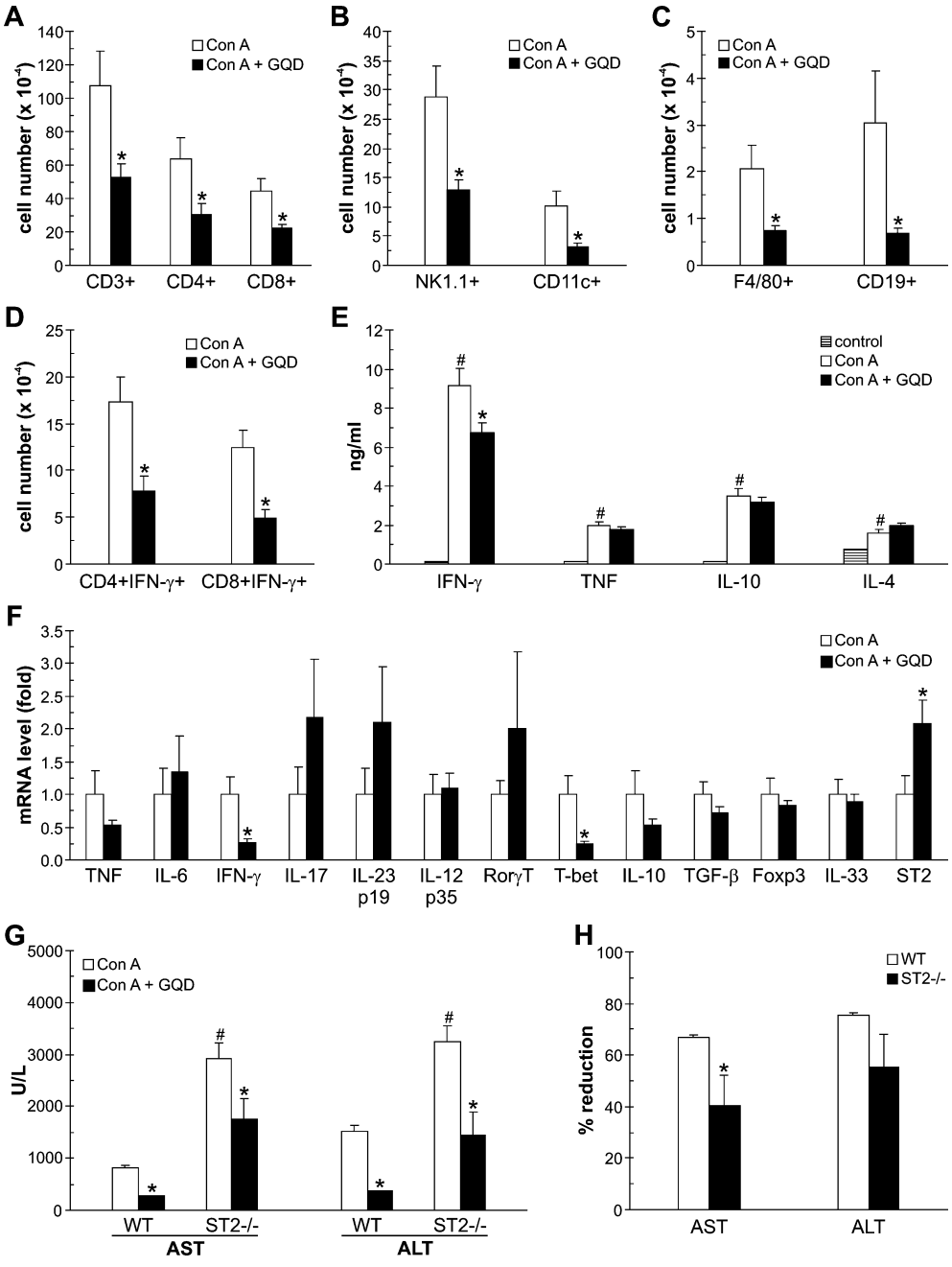

Figure 3. GQDs reduce liver inflammatory infiltration and reduce IFN-γ expression. (A–F) In Con A hepatitis, GQD administration (50 mg/kg) reduces the liver numbers of $CD3^+$ (both $CD4^+$ and $CD8^+$) T cells (A), $NK1.1^+$ NK cells and $CD11c^+$ dendritic cells (B), $F480^+$ macrophages and $CD19^+$ B cells (Figure 3C), as well as IFN-γ-producing $CD4^+$ and $CD8^+$ cells (Figure 3D). Serum levels of IFN-γ (E) and splenocyte expression of IFN-γ mRNA (F) are also reduced by GQD treatment. The liver tissue (A–E) and serum (F) were collected 8 h after Con A injection. The results of one of two experiments with similar results are presented as mean ± SEM values (n = 8 mice per group; p# < 0.05 compared to untreated control; p^* < 0.05 compared to Con A alone). (G, H) GQD injection (50 mg/kg) attenuates Con A-induced liver damage (measured by liver transaminase increase after 24 h) both in WT and $ST2^{-/-}$ mice (G), but the protective effect is less pronounced in ST2-deficient animals (H). The results of one of two experiments with similar results are presented as mean ± SEM values (n = 8 mice per group; $p^{\#}$ < 0.05 compared to WT Con A; p^* < 0.05 compared to corresponding Con A treatment).

other proinflammatory cytokines (TNF, IL-6, IL-12, IL-17, IL-23), anti-inflammatory cytokines (IL-10, TGF-β), and T cell transcription factors (RORγT, Foxp3) was not significantly changed (Figure 3F). It has recently been reported that intravenous application of graphene nanosheets induces Th2 inflammatory response through activation of IL-33/ST2 axis.[24] In agreement with this finding, GQD administration increased the expression of ST2 mRNA in the spleen, although the mRNA level of the ST2 ligand IL-33 was not significantly altered (Figure 3F). ST2 deficiency results in upregulation of IFN-γ production and more severe liver damage after Con A administration,[48] as confirmed in the present study by the increase in liver transaminases (Figure 3G).

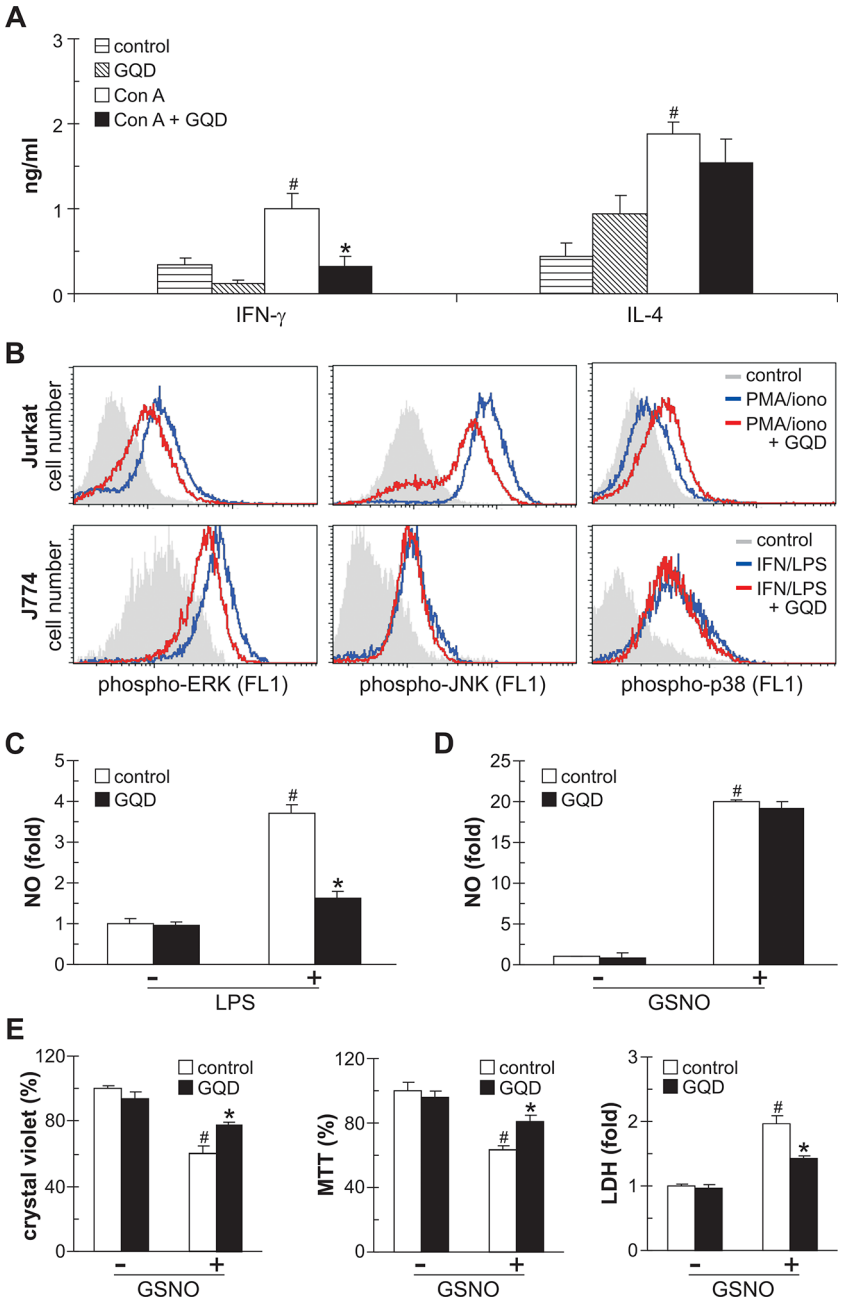

Figure 4. GQDs inhibit macrophage/T cell activation and NO cytotoxicity *in vitro*. (A) GQDs (100 μg/mL) inhibit IFN-γ, but not IL-4 production, in mouse splenocytes stimulated with Con A (5 μg/mL) for 24 h. (B) GQDs (100 μg/mL) modulate MAPK activity in PMA (50 nM) + ionomycin (500 nM)-activated Jurkat T cells (10 min) and IFN-γ (50 ng/mL) + LPS (5 μg/mL)-activated J774 macrophages (30 min). (C) GQDs (100 μg/mL) inhibit NO production in J774 macrophages stimulated with IFN-γ + LPS for 24 h. (D) GQDs (100 μg/mL) do not affect 24 h NO release by NO-donor GSNO (1 mM). (E) GQDs (100 μg/mL) increase the cell numbers (crystal violet assay), improve mitochondrial dehydrogenase activity (MTT test) and reduce cell membrane damage (LDH release assay) in HepG2 cells exposed to GSNO (1 mM) for 24 h. The results are presented as (A) mean ± SEM values from one of two experiments with similar results (n = 8 mice per group; *$p < 0.05$), (B) representative flow cytometry histograms from three independent experiments, or (C−E) mean ± SEM values of triplicates from a representative of three independent experiments ($p^{\#} < 0.05$ and $p^{*} < 0.05$ compared to control cells without and with GSNO, respectively).

While GQDs reduced the serum AST/ALT levels both in wild-type (WT) mice and those lacking the ST2 gene (Figure 3G), the decrease in ALT was significantly less pronounced in ST2-deficient ($ST2^{-/-}$) animals (Figure 3H), and a similar tendency ($p = 0.125$) was observed with ALT (Figure 3H). These data indicate that ST2 upregulation could be partly involved in the hepatoprotective action of GQDs, which is consistent with the role of ST2 signaling in the inhibition of Th1 response-associated inflammation and macrophage activation.[49,50] It should be noted, however, that the observed effects of GQDs on splenocytes seem to contradict the finding that no GQD-specific Raman signal was recorded in spleen lysates (Supporting Information, Figure 1). It is possible

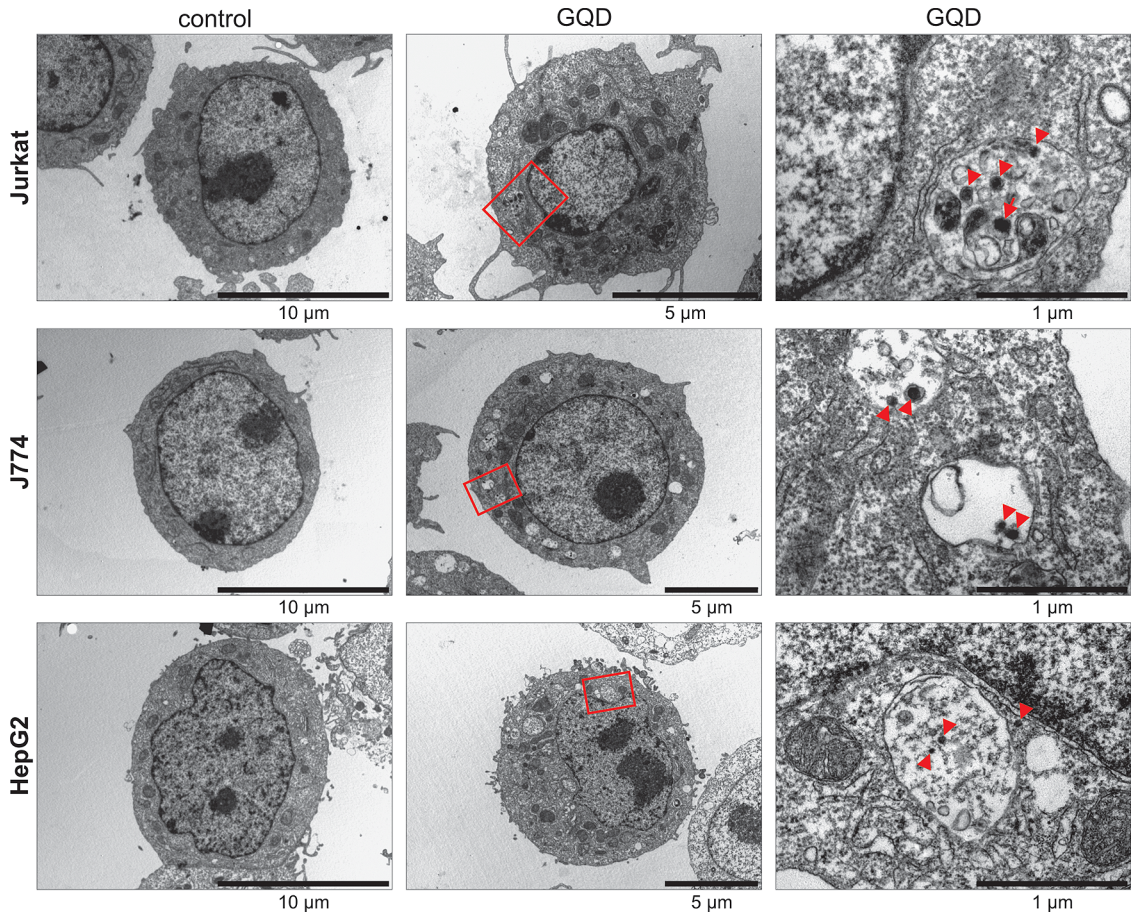

Figure 5. Cellular uptake of GQDs. Representative TEM images of Jurkat, J774, and HepG2 cells treated withs GQDs (100 μg/mL, 1 h) are shown. The arrowheads point at single GQD (diameter 20−70 nm), while arrow points at a larger GQD aggregate.

that the accumulation of GQDs in the spleen was below the detection threshold of Raman spectroscopy but still sufficient to affect the immune response. This seems conceivable if, for example, the observed immunomodulatory effects were mediated by GQD-loaded blood immune cells (*e.g.*, monocytes, dendritic cells) that have migrated to spleen. Our hypothesis is consistent with the recent photoluminescence measurements showing a higher accumulation of intravenously injected GQDs in the mouse liver compared to spleen.[28−30]

We next performed a set of *in vitro* experiments to get some further insight into the cellular and molecular mechanisms of GQD-mediated protection from inflammatory hepatitis. In accordance with the *in vivo* results, spleen mononuclear cells stimulated with Con A secreted less IFN-γ, but not IL-4, when exposed to GQDs (Figure 4A). We also assessed if GQDs could directly modulate the activation of T cells and macrophages by measuring the phosphorylation status of mitogen-activated protein kinases (MAPK), the enzyme family involved in the intracellular signaling in immune cells.[51,52] The flow cytometric analysis of activation in phorbol myristate acetate (PMA) + ionomycin-stimulated Jurkat T cell line revealed that GQDs reduced the phosphorylation of extracellular signal regulated kinase (ERK) and c-Jun N-terminal kinase (JNK) but increased the phosphorylation of p38 MAPK (Figure 4B). In the J774 macrophage cell line stimulated with IFN-γ and *E. coli* lipopolisaccharide (LPS), GQDs inhibited the activation of ERK but not JNK or p38 MAPK (Figure 4B). The activation of MAPK in either Jurkat or J774 cells was not affected by GQDs alone (data not shown). The production of the hepatotoxic free radical nitric oxide (NO),[53] which is apparently involved in Con A hepatitis,[54] was suppressed by GQDs in IFN-γ + LPS-activated J774 macrophages (Figure 4C). The observed effect was not due to the quenching of NO, as GQDs were unable to affect the levels of nitrite, an end product of NO, in the solution of NO donor S-nitrosoglutathione (GSNO) (Figure 4D). Despite the lack of NO-quenching ability, GQDs reduced the toxicity of GSNO toward HepG2 human hepatocyte cell line, as indicated by a significant increase in cell number (crystal violet assay) and mitochondrial dehydrogenase activity (MTT assay), as well as by a decrease in cell membrane damage measured by lactate dehydrogenase (LDH) release (Figure 4E). The observed effects were associated with GQD uptake by Jurkat, J774, and HepG2 cells, as TEM analysis confirmed their presence in the single-membrane

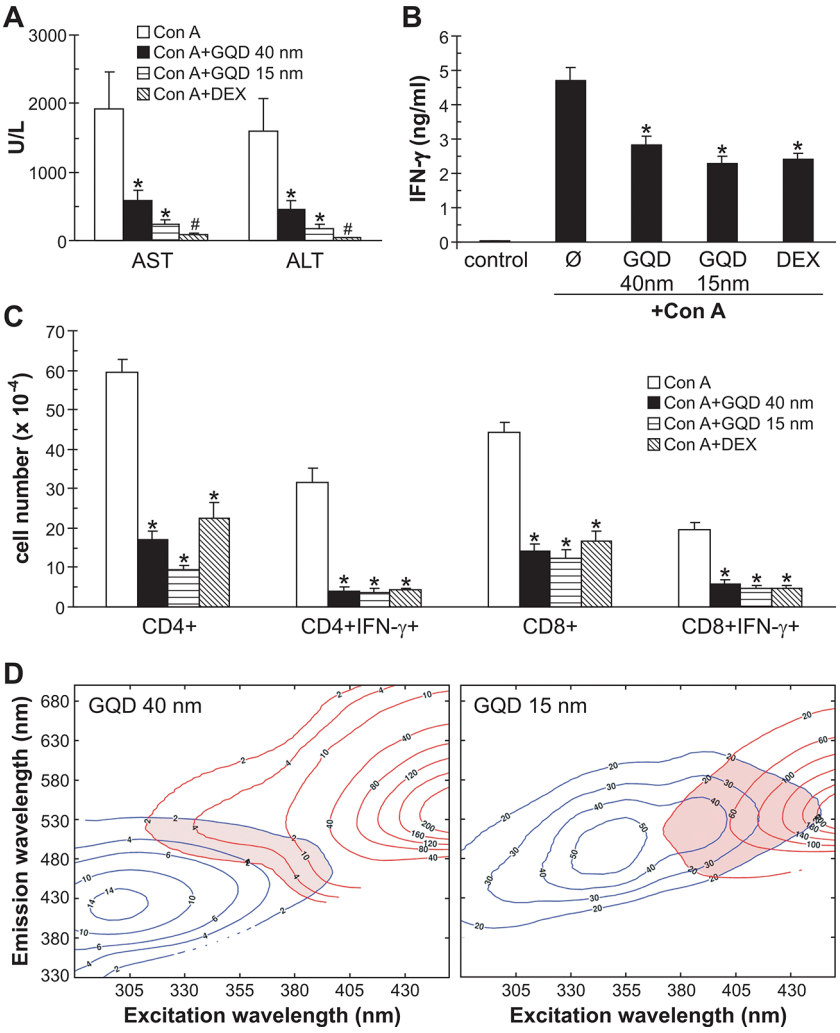

Figure 6. Hepatoprotective effect and urine elimination of small GQDs. (A–C) Small GQDs (15 nm; 50 mg/kg i.v.) were compared with large GQDs (40 nm; 50 mg/kg i.v.) and the conventional immunosuppresant dexamethasone (0.5 mg/kg i.v.) for their ability to reduce serum transaminase (A) and IFN-γ levels (B), as well as liver infiltration of IFN-γ-producing CD4$^+$ and CD8$^+$ T cells (C). The results are presented as mean $\pm$ SEM values (n = 8 mice per group; p^* < 0.05 compared to Con A alone $p^\#$ < 0.05 compared to all other treatments). (D) EEM contour maps (after removing Rayleigh scattering) of GQDs (blue lines) and the urine of mice treated with GQDs (red lines). The shaded region highlights the overlap of GQDs and urine emission.

cytoplasmic vesicles and, less frequently, in the cytoplasm (Figure 5). These data demonstrate that internalization of GQDs interferes with T cell/macrophage MAPK signaling and NO production in macrophages but also directly protects hepatocytes from NO-mediated killing.

Large nanoparticles, such as 40 nm GQDs used here, are mainly eliminated through the liver, either by hepatocytes *via* the biliary system or by phagocytic Kupfer cells.[25] Smaller nanoparticles, on the other hand, are more likely to be excreted in urine, thus enabling fast elimination from the body and preventing excessive accumulation in organs and tissues. Thus, we wanted to explore if the reduction in GQD size could increase their elimination through urine while preserving their hepatoprotective effect. To that end, we used hydrogen peroxide etching to prepare smaller GQDs of 15 nm average length (5–30 nm) and 2 nm average height, corresponding to two graphene layers (Supporting Information, Figure S3). The photoluminescence and Raman spectra of small GQDs were similar to those of the larger ones, and the GQDs readily accumulated in the mouse liver after intravenous injection (Supporting Information, Figure S3), but were undetectable in spleen, lungs, brain or kidney (Supporting Information, Figure S4). The protective effect of small GQDs in Con A hepatitis, measured as a reduction in AST/ALT serum levels, was somewhat but not significantly more pronounced than that of their larger counterparts, while both GQDs were significantly less efficient than the well-known immunosuppressive agent dexamethasone (Figure 6A). The immunomodulatory effects (reduction in IFN- γ serum levels and liver infiltration of IFN-γ -producing CD4$^+$ and CD8$^+$ T cells) were comparable in all three treatments (Figure 6B,C), indicating that the higher

hepatoprotective efficiency of dexamethasone probably stems from its wider immunosuppresive spectrum. The hepatoprotective effect of small GQDs was further supported by histopathological analysis, demonstrating less severe tissue damage and reduced inflammatory infiltration in GQD-treated mice (Supporting Information, Figure S5). In addition, the ability of small GQDs to gain access to intracellular space was confirmed by TEM (Supporting Information, Figure S6). The parallel factor analysis (PARAFAC) of excitation–emission matrices (EEM) obtained by luminescence measurements of urine samples demonstrated that small GQDs were better eliminated through urine than larger GQDs, reaching a markedly higher urine concentration (0.15 vs. 0.013 mg/mL) after intravenous injection (Figure 6D). However, this amount corresponded to less than 20% of the injected GQD dose, indicating that the majority of small GQDs, consistent with the observed hepatoprotection, still accumulated in the liver. The inability of Raman spectroscopy to detect any GQDs in the kidneys (Supporting Information, Figure S4D) could be due to a high internal tissue fluorescence and/or time kinetics of GQD biodistribution. Therefore, while large (40 nm) and small (15 nm) GQDs are both similarly efficient and only slightly less protective in the immune hepatitis than the commercial immunosuppressive agent dexamethasone, smaller GQDs might have the advantage of being better eliminated through urine.

Finally, there is an issue of the toxicity possibly associated with GQD treatment. Several recent reports emphasized the high biocompatibility and the absence of toxic effects of GQDs applied at the concentrations up to 20 mg/kg.[28−30] While the dose in the present study (50 mg/kg) was 2.5-fold higher, it should be noted that we used a single injection, as opposed to a repeated administration (every other day for 14 days) in the report by Chong *et al.*[28] Moreover, a recent study demonstrated that 50 mg/kg of dextran-coated graphene oxide nanoparticles, as another form of graphene, neither displayed any effects in terms of mortality, histopathological findings, respiratory, or cardiovascular safety parameters nor adversely affected the immune system or induced an inflammatory response.[62] In our experiments, no increase in liver transaminases was observed when GQDs were administered alone (Figure 2A), indicating the absence of hepatotoxicity. In addition, the liver and kidney tissue architecture was preserved 24 h after GQD administration (Supporting Information, Figure S7), and no general signs of acute toxicity (respiratory distress, impaired body weight gain, anorexia, weakness, apathy, and death) were observed during 1 week following GQD injection. Nevertheless, more detailed studies on the possible adverse side effects of GQDs are required.

CONCLUSION

Our data demonstrate that GQDs alleviate immune-mediated fulminant hepatitis by reducing hepatic inflammation, oxidative stress, apoptosis, and autophagy. The observed effects apparently involved both immunomodulatory action exerted *via* the interference with T cell and macrophage activation, as well as direct hepatoprotective action due to liver accumulation. Further research is warranted to elucidate in more detail the mechanisms underlying the immunomodulatory and hepatoprotective action of GQDs as well as to explore their potential therapeutic use in the immune-mediated organ damage in human disease.

EXPERIMENTAL METHODS

GQD Synthesis, Characterization, and Biodistribution. A stable suspension of GQDs in normal saline (0.9% NaCl) was prepared by electrochemical oxidation of graphite and characterized by AFM, TEM, and photoluminescence spectroscopy as previously described.[32,33] To obtain smaller nanoparticles, 300 mg of GQDs was sonicated in 30 mL of water, 20 mL of ammonia (25%), and 60 mL of hydrogen peroxide.[55] The mixture was reacted at 50 °C for 1 h under vigorous stirring. After rotary evaporation at 60 °C to remove unreacted hydrogen, ammonia, and water, acetone was used as a poor solvent to precipitate and wash the final GQD product. The reaction yield was ~40%. For biodistribution analysis, GQDs were injected intravenously to mice (100 mg/kg), and liver, spleen, and brain were collected after 2 h and lysed in 10% TCA (1:10 w/v). GQDs and tissue lysates from control (saline-injected) and GQD-injected animals were deposited on glass, and the Raman spectra were obtained on a DXR Raman microscope (Thermo Fisher Scientific, Waltham, MA) using a 532 nm excitation line from a diode-pumped, solid-state laser (5 mW). The Raman spectra were recorded with an 1800 lines/mm grating, using 50× objectives to focus the excitation laser light. The spot of the laser beam was 0.7 μm, the spectral resolution was 0.5 cm^{-1}, and the acquisition time was 100 (10 × 10) s. Ten Raman spectra of each sample were recorded at different areas of the sample.

Luminescence Measurements of GQD Urine Concentration. Urine samples were collected after 24 h from mice intravenously injected with saline or GQDs (100 mg/kg). EEM were measured on a PerkinElmer fluorescence spectrophotometer LS45 at room temperature in the right angle geometry. EEM were obtained by recording the emission spectra (from 330 to 680 at 0.5 nm intervals) corresponding to excitation wavelengths ranging between 280 and 450 nm (with a 5 nm step) and automatically normalized to the excitation intensity by the instrument. Fluorescence data were analyzed by PARAFAC[56,57] using the Solo Version 6.5.4 software package (eigenvector Research Inc., Wenatchee, WA). PARAFAC was calibrated with EEM measurements on water solutions of GQDs of 0.01 to 0.50 mg/mL concentrations.

Con A Hepatitis and GQD Treatment. For the induction of Con A hepatitis, we used 6–8 week old male WT and $ST2^{-/-}$ BALB/c mice,[48] kindly provided by Professor F. Y. Liew (University of Glasgow, UK), maintained in our animal facility. All experiments were approved by the Animal Ethics Committee of Faculty of Medicine (Kragujevac, Serbia) and performed according to the criteria outlined in the "Guide for the Care and Use of Laboratory Animals" (NIH publication 86-23, revised 1985). For the hepatitis induction, mice were given a single intravenous injection of Con A (Sigma-Aldrich, St. Louis, MO) at 12 mg/kg of body

weight in 250 μL of saline. GQDs (50 mg/kg) were given in 500 μL saline 30 min before Con A, while control animals received the appropriate amount of saline only. The livers and spleens for the flow cytometry, immunoblot and RT-PCR analysis, as well as sera for cytokine measurement, were collected 8 h after Con A injection, while the liver tissue for histological analysis was collected 24 h after Con A administration. Serum levels of AST and ALT were measured 24 h after Con A administration using the automated biochemistry analyzer Olympus AU 400 (Olympus Diagnostica GMBH, Hamburg, Germany).

Histopathology and Lipid Peroxidation. The histopathological analysis of liver tissue was performed as previously described.[48] The lipid peroxide content in liver tissue was determined by thiobarbituric acid reaction as previously reported.[58]

Flow Cytometry Analysis of Cell Populations and MAPK Signaling. Splenocytes and liver-infiltrating mononuclear cells were isolated, and flow cytometry analysis of cell populations was performed as previously described.[48,59] The phosphorylation of ERK, JNK, and p38 MAPK in human Jurkat T cell line (ATCC TIB-152) and J774.1 mouse macrophage cell line (ATCC TIB-67) was assessed by phospho-flow cytometry. Jurkat or J774 cells (10^6/mL) were incubated for 1 h with GQDs (100 μg/mL) in the flow cytometry tubes in a HEPES (20 mM)-buffered RPMI 1640 medium supplemented with 10% fetal bovine serum (FBS), 2 mM L-glutamine, and 1% of antibiotic/antimycotic mixture (all from PAA, Pasching, Austria) (cell culture medium). Jurkat cells were then stimulated for 10 min with PMA (50 nM) + ionomycin (500 nM), while J774 cells were stimulated with IFN-γ (50 ng/mL) and *E. coli* LPS (5 μg/mL) (all from Sigma-Aldrich, St. Louis, MO) for 30 min. Cells were then fixed with 2% paraformaldehyde, incubated at 37 °C for 10 min, and washed (400 g, 5 min, 4 °C) in ice-cold staining buffer (PBS, 1% FBS, 1 mM EDTA). Cells were permeabilized by ice-cold methanol on ice for 30 min, washed two times in staining buffer, and incubated at 25 °C for 30 min with rabbit antibodies (Cell Signaling Technology, Cambridge, MA) against phospho-ERK (Cat. No. 9101), phospho-JNK (9251), phospho-p38 (9211) (all at 0.4 μg/mL final concentration), or appropriate isotype control antibody. After being washed in staining buffer, cells were incubated for 30 min with secondary antirabbit IgG-AlexaFluor 488 antibody (0.4 μg/mL; Cell Signaling Technology, Cambridge, MA), washed, and analyzed on a FACSCalibur flow cytometer (BD Bioscience, Heidelberg, Germany) using CellQuest software.

Real-Time RT-PCR Analysis of Apoptosis- and Autophagy-Related Genes. Total RNA was extracted using TRIZOL and reverse transcribed with M-MuLV reverse transcriptase and random hexamers (all from Life Technologies, Carlsbad, CA). The real time RT-PCR analysis was performed in a Realplex Mastercycler (Eppendorf, Hamburg, Germany) using TaqMan Master Mix and the following TaqMan primers and probes from Life Technologies (Carlsbad, CA): Atg4b (catalog no. Mm00558047_m1), Atg5 (Mm00504340_m1), Atg7 (Mm00512209_m1), Atg12 (Mm00503201_m1), γ-aminobutyric acid receptor-associated protein (Gabarap; Mm00490678_m1), beclin-1 (Mm01265461_m1), p21/Waf1 (Mm00432448_m1), p27/Kip1 (Mm00438168_m1), p53-upregulated modulator of apoptosis (Puma; Mm00519268_m1), Noxa (Mm00451763_m1), B-cell lymphoma 2 (Bcl-2; Mm00477631_m1), Bcl-2-associated X protein (Bax; Mm00432051_m1), Bcl-2-associated death promoter (Bad; Mm00432042_m1), Bcl-2 homologous antagonist killer 1 (Bak1; Mm00432045_m1), B-cell lymphoma 2 interacting mediator of cell death (Bim; Mm00437796_m1), p53 (Mm01731287_m1), phosphatase and tensin homologue (Pten; Mm00477208_m1), apoptotic protease activating factor 1 (Apaf1; Mm01223702_m1), Bcl-xL (Mm00437783_m1), X-linked inhibitor of apoptosis protein (XIAP; Mm00776505_m1), survivin (Mm00599749_m1), TNF (Mm0043258_m1), IL-6 (Mm00446190_m1), IFN-γ (Mm01168134_m1), IL-17A (Mm00439618_m1), IL-23 p19 (Mm01160011_g1), IL-12p35 (Mm00434165_m1), RORγt (Mm01261022_m1), T-bet (Mm00450960_m1), IL-10 (Mm00439614_m1), TGF-β (Mm01178820_m1), Foxp3 (Mm00475162_m1), IL-33 (Mm00505403_m1), ST2 (Mm00516117_m1), and 18s RNA (Mm03928990_g1). The reaction conditions were as recommended by the manufacturer. The threshold cycle (Ct) values of the housekeeping gene (18s RNA) were subtracted from Ct values of target genes to obtain ΔCt. The relative gene expression is presented as $2^{-\Delta Ct}$ value normalized to the treatment without GQDs.

Immunoblot Analysis of Apoptosis and Autophagy. Tissue samples were homogenized in lysis buffer (30 mM Tris-HCl pH 8.0, 150 mM NaCl, 1% NP-40) containing 1 mM phenylmethylsulfonyl fluoride, 1 mM Na vanadate, 10 mM NaF, and protease inhibitor cocktail (all from Sigma-Aldrich, St. Louis, MO) on ice for 30 min and centrifuged at 14000*g* for 15 min at 4 °C, and the supernatants were collected. Equal amounts of protein from each sample were separated by SDS-PAGE and transferred to nitrocellulose membranes (Bio-Rad, Hemel Hempstead, UK). Following incubation with primary rabbit antibodies (Cell Signaling Technology, Cambridge, MA) against caspase-3 (#9665), PARP (#9532), LC3β (#2775) or actin (#4968), and peroxidase-conjugated goat antirabbit IgG (#7074) as a secondary antibody, specific protein bands were visualized using enhanced chemiluminescence reagent (GE Healthcare, Pollards Wood, UK).

Cytokine Measurement. The levels of IFN-γ, TNF, IL-10, and IL-4 in mouse sera and 24 h supernatants of Con A (5 μg/mL)-stimulated splenocytes (10^6/well in 24-well plate) were measured using ELISA kits (R&D Systems, Minneapolis, MN) according to the manufacturer's instructions.

NO Production. J774 cells (10^4/well, 96-well plate) were incubated overnight in cell culture medium. Afterward, cells were incubated for 30 min with GQDs (100 μg/mL) and then stimulated with IFN-γ (50 ng/mL) and LPS (5 μg/mL) for 24 h. Alternatively, GQDs (100 μg/mL) were incubated in cell culture medium with NO donor GSNO. NO production was assessed by measuring the concentration of nitrite as an end-product of NO by Griess reaction, as previously described.[60]

Cell Viability. Human hepatocarcinoma cells HepG2 (ATCC HB-8065) were incubated overnight (2×10^4/well, 96-well plate) in cell culture medium. Afterward, cells were incubated for 30 min with GQDs (100 μg/mL) and then treated for an additional 24 h with 1 mM of NO-releasing compound GSNO (Sigma-Aldrich, St. Louis, MO). Cell viability was determined as previously described[61] by measuring cell numbers, mitochondrial dehydrogenase activity, and cell membrane damage using crystal violet staining, MTT test, and LDH release assay, respectively.

TEM Analysis of GQD Cellular Internalization. Jurkat T cells, J774 macrophages, and HepG2 hepatocytes (3×10^6 in a 100 mm Petri dish) were incubated overnight in cell culture medium and then treated with GQDs (100 μg/mL). After 1 h, cells were fixed with 3% glutaraldehyde in cacodylate buffer, postfixed in 1% osmium tetraoxide, dehydrated in graded alcohols, and then embedded in Epon 812. The ultrathin sections were stained in uranyl acetate and lead citrate and were examined using a Morgagni 268D electron microscope (FEI, Hillsboro, OR).

Statistical Analysis. Results were analyzed using t-test or one-way ANOVA followed by a Student−Newman−Keuls test for multiple comparisons. All data were expressed as the mean ± SEM, and the values of $p < 0.05$ were considered as statistically significant.

Conflict of Interest: The authors declare no competing financial interest.

Supporting Information Available: Biodistribution of GQDs, immunomodulatory effects of GQDs in Con A hepatitis, characterization and liver accumulation of small GQDs, biodistribution of small GQDs, effect of small GQDs on Con A-induced liver damage and inflammatory infiltration, cellular uptake of small GQDs, histopathological analysis of liver and kidneys from GQD-treated mice. This material is available free of charge *via* the Internet at http://pubs.acs.org

Acknowledgment. This study was supported by Grant Nos. 41025, 175069, 175103, 172003, and 173053 from the Ministry of Education, Science and Technological Development, Republic of Serbia, and MP01/12 from The Faculty of Medical Sciences University of Kragujevac, Serbia. The authors thank

Merck KGaA (Darmstadt, Germany) for providing PCR equipment and reagents.

REFERENCES AND NOTES

1. Bitounis, D.; Ali-Boucetta, H.; Hong, B. H.; Min, D. H.; Kostarelos, K. Prospects and Challenges of Graphene in Biomedical Applications. *Adv. Mater.* **2013**, *25*, 2258–2268.
2. Kostarelos, K.; Novoselov, K. S. Materials Science. Exploring the Interface of Graphene and Biology. *Science* **2014**, *344*, 261–263.
3. Mao, H. Y.; Laurent, S.; Chen, W.; Akhavan, O.; Imani, M.; Ashkarran, A. A.; Mahmoudi, M. Graphene: Promises, Facts, Opportunities, and Challenges in Nanomedicine. *Chem. Rev.* **2013**, *113*, 3407–3424.
4. Ponomarenko, L. A.; Schedin, F.; Katsnelson, M. I.; Yang, R.; Hill, E. W.; Novoselov, K. S.; Geim, A. K. Chaotic Dirac Billiard in Graphene Quantum Dots. *Science* **2008**, *320*, 356–358.
5. Li, L.; Wu, G.; Yang, G.; Peng, J.; Zhao, J.; Zhu, J. J. Focusing on Luminescent Graphene Quantum Dots: Current Status and Future Perspectives. *Nanoscale* **2013**, *5*, 4015–4039.
6. Shen, J.; Zhu, Y.; Yang, X.; Li, C. Graphene Quantum Dots: Emergent Nanolights for Bioimaging, Sensors, Catalysis and Photovoltaic Devices. *Chem. Commun. (Cambridge)* **2012**, *48*, 3686–3699.
7. Wang, X.; Cao, L.; Lu, F.; Meziani, M. J.; Li, H.; Qi, G.; Zhou, B.; Harruff, B. A.; Kermarrec, F.; Sun, Y. P. Photoinduced Electron Transfers With Carbon Dots. *Chem. Commun. (Cambridge)* **2009**, *25*, 3774–3776.
8. Christensen, I. L.; Sun, Y. P.; Juzenas, P. Carbon Dots as Antioxidants and Prooxidants. *J. Biomed. Nanotechnol.* **2011**, *7*, 667–676.
9. Yang, Y.; Bazhin, A. V.; Werner, J.; Karakhanova, S. Reactive Oxygen Species in the Immune System. *Int. Rev. Immunol.* **2013**, *32*, 249–270.
10. Sena, L. A.; Li, S.; Jairaman, A.; Prakriya, M.; Ezponda, T.; Hildeman, D. A.; Wang, C. R.; Schumacker, P. T.; Licht, J. D.; Perlman, H.; et al. Mitochondria Are Required for Antigen-Specific T Cell Activation Through Reactive Oxygen Species Signaling. *Immunity* **2013**, *38*, 225–236.
11. Kaminski, M. M.; Sauer, S. W.; Klemke, C. D.; Süss, D.; Okun, J. G.; Krammer, P. H.; Gülow, K. Mitochondrial Reactive Oxygen Species Control T Cell Activation by Regulating IL-2 and IL-4 Expression: Mechanism of Ciprofloxacin-Mediated Immunosuppression. *J. Immunol.* **2010**, *184*, 4827–4841.
12. Ahsan, H.; Ali, A.; Ali, R. Oxygen Free radicals and Systemic Autoimmunity. *Clin. Exp. Immunol.* **2003**, *131*, 398–404.
13. Noubade, R.; Wong, K.; Ota, N.; Rutz, S.; Eidenschenk, C.; Valdez, P. A.; Ding, J.; Peng, I.; Sebrell, A.; Caplazi, P.; *et al.* NRROS Negatively Regulates Reactive Oxygen Species During Host Defence and Autoimmunity. *Nature* **2014**, *509*, 235–239.
14. Jaeschke, H. Reactive Oxygen and Mechanisms of Inflammatory Liver Injury: Present Concepts. *J. Gastroenterol. Hepatol.* **2011**, *26*, 173–179.
15. Mitchell, L. A.; Lauer, F. T.; Burchiel, S. W.; McDonald, J. D. Mechanisms for How Inhaled Multiwalled Carbon Nanotubes Suppress Systemic Immune Function in Mice. *Nat. Nanotechnol.* **2009**, *4*, 451–456.
16. Mitchell, L. A.; Gao, J.; Wal, R. V.; Gigliotti, A.; Burchiel, S. W.; McDonald, J. D. Pulmonary and Systemic Immune Response to Inhaled Multiwalled Carbon Nanotubes. *Toxicol. Sci.* **2007**, *100*, 203–214.
17. Ryan, J. J.; Bateman, H. R.; Stover, A.; Gomez, G.; Norton, S. K.; Zhao, W.; Schwartz, L. B.; Lenk, R.; Kepley, C. L. Fullerene Nanomaterials Inhibit the Allergic Response. *J. Immunol.* **2007**, *179*, 665–672.
18. Yang, D.; Zhao, Y.; Guo, H.; Li, Y.; Tewary, P.; Xing, G.; Hou, W.; Oppenheim, J. J.; Zhang, N. $[Gd@C_{82}(OH)_{22}]_n$ Nanoparticles Induce Dendritic Cell Maturation and Activate Th1 Immune Responses. *ACS Nano* **2010**, *4*, 1178–1186.
19. Zogovic, N. S.; Nikolic, N. S.; Vranjes-Djuric, S. D.; Harhaji, L. M.; Vucicevic, L. M.; Janjetovic, K. D.; Misirkic, M. S.; Todorovic-Markovic, B. M.; Markovic, Z. M.; Milonjic, S. K.; *et al.* Opposite Effects of Nanocrystalline Fullerene (C_{60}) on Tumour Cell Growth *In Vitro* and *In Vivo* and a Possible Role of Immunosupression in the Cancer-Promoting Activity of C_{60}. *Biomaterials* **2009**, *30*, 6940–6946.
20. Delogu, L. G.; Venturelli, E.; Manetti, R.; Pinna, G. A.; Carru, C.; Madeddu, R.; Murgia, L.; Sgarrella, F.; Dumortier, H.; Bianco, A. *Ex Vivo* Impact of Functionalized Carbon Nanotubes on Human Immune Cells. *Nanomedicine (London)* **2012**, *7*, 231–243.
21. Pescatori, M.; Bedognetti, D.; Venturelli, E.; Menard-Moyon, C.; Bernardini, C.; Muresu, E.; Piana, A.; Maida, G.; Manetti, R.; Sgarrella, F.; *et al.* Functionalized Carbon Nanotubes as Immunomodulator Systems. *Biomaterials* **2013**, *34*, 4395–4403.
22. Tkach, A. V.; Shurin, G. V.; Shurin, M. R.; Kisin, E. R.; Murray, A. R.; Young, S. H.; Star, A.; Fadeel, B.; Kagan, V. E.; Shvedova, A. A. Direct Effects of Carbon Nanotubes on Dendritic Cells Induce Immune Suppression Upon Pulmonary Exposure. *ACS Nano* **2011**, *5*, 5755–5762.
23. Tkach, A. V.; Yanamala, N.; Stanley, S.; Shurin, M. R.; Shurin, G. V.; Kisin, E. R.; Murray, A. R.; Pareso, S.; Khaliullin, T.; Kotchey, G. P.; *et al.* Graphene Oxide, but Not Fullerenes, Targets Immunoproteasomes and Suppresses Antigen Presentation by Dendritic Cells. *Small* **2013**, *9*, 1686–1690.
24. Wang, X.; Podila, R.; Shannahan, J. H.; Rao, A. M.; Brown, J. M. Intravenously Delivered Graphene Nanosheets and Multiwalled Carbon Nanotubes Induce Site-Specific Th2 Inflammatory Responses *Via* the IL-33/ST2 Axis. *Int. J. Nanomed.* **2013**, *8*, 1733–1748.
25. Longmire, M.; Choyke, P. L.; Kobayashi, H. Clearance Properties of Nano-Sized Particles and Molecules as Imaging Agents: Considerations and Caveats. *Nanomedicine (London)* **2008**, *3*, 703–717.
26. Sarin, H. Physiologic Upper Limits of Pore Size of Different Blood Capillary Types and Another Perspective on the Dual Pore Theory of Microvascular Permeability. *Angiogenes. Res.* **2010**, *2*, 14.
27. Rizzo, L. Y.; Theek, B.; Storm, G.; Kiessling, F.; Lammers, T. Recent Progress in Nanomedicine: Therapeutic, Diagnostic and Theranostic Applications. *Curr. Opin. Biotechnol.* **2013**, *24*, 1159–1166.
28. Chong, Y.; Ma, Y.; Shen, H.; Tu, X.; Zhou, X.; Xu, J.; Dai, J.; Fan, S.; Zhang, Z. The *In Vitro* and *In Vivo* Toxicity of Graphene Quantum Dots. *Biomaterials* **2014**, *35*, 5041–5048.
29. Nurunnabi, M.; Khatun, Z.; Huh, K. M.; Park, S. Y.; Lee, D. Y.; Cho, K. J.; Lee, Y. K. *In Vivo* Biodistribution and Toxicology of Carboxylated Graphene Quantum Dots. *ACS Nano* **2013**, *7*, 6858–6867.
30. Abdullah-Al-Nahain; Lee, J. E.; In, I.; Lee, H.; Lee, K. D.; Jeong, J. H.; Park, S. Y. Target Delivery and Cell Imaging Using Hyaluronic Acid-Functionalized Graphene Quantum Dots. *Mol. Pharmaceutics* **2013**, *10*, 3736–344.
31. Nurunnabi, M.; Khatun, Z.; Nafiujjaman, M.; Lee, D. G.; Lee, Y. K. Surface Coating of Graphene Quantum Dots Using Mussel-Inspired Polydopamine for Biomedical Optical Imaging. *ACS Appl. Mater. Interfaces* **2013**, *5*, 8246–8253.
32. Markovic, Z. M.; Ristic, B. Z.; Arsikin, K. M.; Klisic, D. G.; Harhaji-Trajkovic, L. M.; Todorovic-Markovic, B. M.; Kepic, D. P.; Kravic-Stevovic, T. K.; Jovanovic, S. P.; Milenkovic, M. M.; et al. Graphene Quantum Dots as Autophagy-Inducing Photodynamic Agents. *Biomaterials* **2012**, *33*, 7084–7092.
33. Ristic, B. Z.; Milenkovic, M. M.; Dakic, I. R.; Todorovic-Markovic, B. M.; Milosavljevic, M. S.; Budimir, M. D.; Paunovic, V. G.; Dramicanin, M. D.; Markovic, Z. M.; Trajkovic, V. S. Photodynamic Antibacterial Effect of Graphene Quantum Dots. *Biomaterials* **2014**, *35*, 4428–4435.
34. Sun, Y. P.; Zhou, B.; Lin, Y.; Wang, W.; Fernando, K. A.; Pathak, P.; Meziani, M. J.; Harruff, B. A.; Wang, X.; Wang, H.; et al. Quantum-Sized Carbon Dots for Bright and Colorful Photoluminescence. *J. Am. Chem. Soc.* **2006**, *128*, 7756–7757.
35. Malard, L. M.; Pimenta, M. A.; Dresselhaus, G.; Dresselhaus, M. S. Raman Spectroscopy in Graphene. *Phys. Rep.* **2009**, *473*, 51–87.

36. Santodomingo-Garzon, T.; Swain, M. G. Role of NKT Cells in Autoimmune Liver Disease. *Autoimmun. Rev.* **2011**, *10*, 793–800.
37. Tiegs, G.; Hentschel, J.; Wendel, A. A T Cell-Dependent Experimental Liver Injury in Mice Inducible by Concanavalin A. *J. Clin. Invest.* **1992**, *90*, 196–203.
38. Wang, H. X.; Liu, M.; Weng, S. Y.; Li, J. J.; Xie, C.; He, H. L.; Guan, W.; Yuan, Y. S.; Gao, J. Immune Mechanisms of Concanavalin A Model of Autoimmune Hepatitis. *World J. Gastroenterol.* **2012**, *18*, 119–125.
39. Draper, H. H.; Hadley, M. Malondialdehyde Determination as Index of Lipid Peroxidation. *Methods Enzymol.* **1990**, *186*, 421–431.
40. Jain, M. V.; Paczulla, A. M.; Klonisch, T.; Dimgba, F. N.; Rao, S. B.; Roberg, K.; Schweizer, F.; Lengerke, C.; Davoodpour, P.; Palicharla, V. R.; *et al.* Interconnections Between Apoptotic, Autophagic and Necrotic Pathways: Implications for Cancer Therapy Development. *J. Cell. Mol. Med.* **2013**, *17*, 12–29.
41. Rautou, P. E.; Mansouri, A.; Lebrec, D.; Durand, F.; Valla, D.; Moreau, R. Autophagy in Liver Diseases. *J. Hepatol.* **2010**, *53*, 1123–1134.
42. Torisu, T.; Nakaya, M.; Watanabe, S.; Hashimoto, M.; Yoshida, H.; Chinen, T.; Yoshida, R.; Okamoto, F.; Hanada, T.; Torisu, K.; *et al.* Suppressor of Cytokine Signaling 1 Protects Mice Against Concanavalin A-Induced Hepatitis by Inhibiting Apoptosis. *Hepatology* **2008**, *47*, 1644–1654.
43. Zhou, F.; Ajuebor, M. N.; Beck, P. L.; Le, T.; Hogaboam, C. M.; Swain, M. G. CD154-CD40 Interactions Drive Hepatocyte Apoptosis in Murine Fulminant Hepatitis. *Hepatology* **2005**, *42*, 372–380.
44. Kaneko, Y.; Harada, M.; Kawano, T.; Yamashita, M.; Shibata, Y.; Gejyo, F.; Nakayama, T.; Taniguchi, M. Augmentation of Vα14 NKT Cell-Mediated Cytotoxicity by Interleukin 4 in an Autocrine Mechanism Resulting in the Development of Concanavalin A-Induced Hepatitis. *J. Exp. Med.* **2000**, *191*, 105–114.
45. Kusters, S.; Gantner, F.; Kunstle, G.; Tiegs, G. Interferon Gamma Plays a Critical Role in T Cell-Dependent Liver Injury in Mice Initiated by Concanavalin A. *Gastroenterology* **1996**, *111*, 462–471.
46. Mullen, A. C.; High, F. A.; Hutchins, A. S.; Lee, H. W.; Villarino, A. V.; Livingston, D. M.; Kung, A. L.; Cereb, N.; Yao, T. P.; Yang, S. Y.; *et al.* Role of T-bet In Commitment of T_H1 Cells Before IL-12-Dependent Selection. *Science* **2001**, *292*, 1907–1910.
47. Szabo, S. J.; Kim, S. T.; Costa, G. L.; Zhang, X.; Fathman, C. G.; Glimcher, L. H. A Novel Transcription Factor, T-bet, Directs Th1 Lineage Commitment. *Cell* **2000**, *100*, 655–669.
48. Volarevic, V.; Mitrovic, M.; Milovanovic, M.; Zelen, I.; Nikolic, I.; Mitrovic, S.; Pejnovic, N.; Arsenijevic, N.; Lukic, M. L. Protective Role of IL-33/ST2 Axis in Con A-Induced Hepatitis. *J. Hepatol.* **2012**, *56*, 26–33.
49. Milovanovic, M.; Volarevic, V.; Radosavljevic, G.; Jovanovic, I.; Pejnovic, N.; Arsenijevic, N.; Lukic, M. L. IL-33/ST2 Axis in Inflammation and Immunopathology. *Immunol. Res.* **2012**, *52*, 89–99.
50. Trajkovic, V.; Sweet, M. J.; Xu, D. T1/ST2 — an IL-1 Receptor-Like Modulator of Immune Responses. *Cytokine Growth Factor Rev.* **2004**, *15*, 87–95.
51. Rincon, M.; Flavell, R. A.; Davis, R. A. The JNK and P38 MAP Kinase Signaling Pathways in T Cell-Mediated Immune Responses. *Free Radic. Biol. Med.* **2000**, *28*, 1328–1337.
52. Symons, A.; Beinke, S.; Ley, S. C. MAP Kinase Kinase Kinases and Innate Immunity. *Trends Immunol.* **2006**, *27*, 40–48.
53. Siendones, E.; Fouad, D.; Abou-Elella, A. M.; Quintero, A.; Barrera, P.; Muntane, J. Role of Nitric Oxide in D-Galactosamine-Induced Cell Death and its Protection by PGE1 in Cultured Hepatocytes. *Nitric Oxide* **2003**, *8*, 133–143.
54. Okamoto, T.; Masuda, Y.; Kawasaki, T.; Shinohara, M.; Matsuzaki, K. Aminoguanidine Prevents Concanavalin A-Induced Hepatitis in Mice. *Eur. J. Pharmacol.* **2000**, *396*, 125–130.
55. Jiang, F.; Chen, D.; Li, R.; Wang, Y.; Zhang, G.; Li, S.; Zheng, J.; Huang, N.; Gu, Y.; Wang, C.; Shu, C. Eco-Friendly Synthesis of Size-Controllable Amine-Functionalized Graphene Quantum Dots with Antimycoplasma Properties. *Nanoscale* **2013**, *5*, 1137–1142.
56. Bro, R. PARAFAC. Tutorial and Applications. *Chemometr. Intell. Lab. Syst.* **1997**, *38*, 149–171.
57. Andersen, C. M.; Bro, R. Practical Aspects of PARAFAC Modeling of Fluorescence Excitation-Emission Data. *J. Chemometr.* **2003**, *17*, 200–215.
58. Losa, G. A. Resveratrol Modulates Apoptosis and Oxidation in Human Blood Mononuclear Cells. *Eur. J. Clin. Invest.* **2003**, *33*, 818–823.
59. Volarevic, V.; Milovanovic, M.; Ljujic, B.; Pejnovic, N.; Arsenijevic, N.; Nilsson, U.; Leffler, H.; Lukic, M. L. Galectin-3 Deficiency Prevents Concanavalin A-Induced Hepatitis in Mice. *Hepatology* **2012**, *55*, 1954–1964.
60. Mijatovic, S.; Maksimovic-Ivanic, D.; Radovic, J.; Popadic, D.; Momcilovic, M.; Harhaji, L.; Miljkovic, D.; Trajkovic, V. Aloe-Emodin Prevents Cytokine-Induced Tumor Cell Death: the Inhibition of Auto-Toxic Nitric Oxide Release as a Potential Mechanism. *Cell. Mol. Life Sci.* **2004**, *61*, 1805–1815.
61. Kaludjerovic, G. N.; Miljkovic, D.; Momcilovic, M.; Djinovic, V. M.; Mostarica Stojkovic, M.; Sabo, T. J.; Trajkovic, V. Novel Platinum(IV) Complexes Induce Rapid Tumor Cell Death *In Vitro*. *Int. J. Cancer* **2005**, *116*, 479–486.
62. Kanakia, S.; Toussaint, J. D.; Mullick Chowdhury, S.; Tembulkar, T.; Lee, S.; Jiang, Y. P.; Lin, R. Z.; Shroyer, K. R.; Moore, W.; Sitharaman, B. Dose Ranging, Expanded Acute Toxicity and Safety Pharmacology Studies for Intravenously Administered Functionalized Graphene Nanoparticle Formulations. *Biomaterials* **2014**, *35*, 7022–7031.